


 Cite this: *Phys. Chem. Chem. Phys.*,  
 2016, 18, 3086

# Flexibility at a glycosidic linkage revealed by molecular dynamics, stochastic modeling, and $^{13}\text{C}$ NMR spin relaxation: conformational preferences of $\alpha$ -L-Rhap- $\alpha$ -(1 $\rightarrow$ 2)- $\alpha$ -L-Rhap-OMe in water and dimethyl sulfoxide solutions

 Robert Pendrill,<sup>a</sup> Olof Engström,<sup>a</sup> Andrea Volpato,<sup>b</sup> Mirco Zerbetto,<sup>b</sup>  
 Antonino Polimeno<sup>\*b</sup> and Göran Widmalm<sup>\*a</sup>

The monosaccharide L-rhamnose is common in bacterial polysaccharides and the disaccharide  $\alpha$ -L-Rhap- $\alpha$ -(1  $\rightarrow$  2)- $\alpha$ -L-Rhap-OMe represents a structural model for a part of *Shigella flexneri* O-antigen polysaccharides. Utilization of [1'- $^{13}\text{C}$ ]-site-specific labeling in the anomeric position at the glycosidic linkage between the two sugar residues facilitated the determination of transglycosidic NMR  $^3J_{\text{CH}}$  and  $^3J_{\text{CC}}$  coupling constants. Based on these spin-spin couplings the major state and the conformational distribution could be determined with respect to the  $\psi$  torsion angle, which changed between water and dimethyl sulfoxide (DMSO) as solvents, a finding mirrored by molecular dynamics (MD) simulations with explicit solvent molecules. The  $^{13}\text{C}$  NMR spin relaxation parameters  $T_1$ ,  $T_2$ , and heteronuclear NOE of the probe were measured for the disaccharide in DMSO- $d_6$  at two magnetic field strengths, with standard deviations  $\leq 1\%$ . The combination of MD simulation and a stochastic description based on the diffusive chain model resulted in excellent agreement between calculated and experimentally observed  $^{13}\text{C}$  relaxation parameters, with an average error of  $< 2\%$ . The coupling between the global reorientation of the molecule and the local motion of the spin probe is deemed essential if reproduction of NMR relaxation parameters should succeed, since decoupling of the two modes of motion results in significantly worse agreement. Calculation of  $^{13}\text{C}$  relaxation parameters based on the correlation functions obtained directly from the MD simulation of the solute molecule in DMSO as solvent showed satisfactory agreement with errors on the order of 10% or less.

 Received 16th October 2015,  
 Accepted 9th December 2015

DOI: 10.1039/c5cp06288h

[www.rsc.org/pccp](http://www.rsc.org/pccp)

## Introduction

Among the biopolymers, nucleic acids, proteins and polysaccharides, the latter are unique in the sense that connections of the monomers may occur with different stereochemistry ( $\alpha$ - or  $\beta$ -glycosidic linkages), at different atomic positions around the sugar ring and its exocyclic groups as well as multi-substitution resulting in branched structures in contrast to the linear sequence of nucleic acids and proteins. It is pertinent to discuss these molecules with respect to their three-dimensional (3D) structures and subsequently their dynamics.<sup>1</sup> Besides the possible permutations described above for carbohydrates, the large number of monosaccharides available (on the order of  $10^3$ ) makes the potential structural glycome huge, and highly

complex oligosaccharides<sup>2,3</sup> and polysaccharides<sup>4</sup> are found in nature where they play important roles in biological systems.<sup>5</sup>

Whereas the monosaccharide D-mannose is present in both human and bacteria, L-rhamnose (6-deoxy-L-mannose) is absent from the former, but quite common among bacteria of different species. It is a constituent of the core region of lipopolysaccharides (LPS),<sup>6</sup> the backbone of O-antigen polysaccharides of LPS,<sup>7–11</sup> and also in side-chains of polysaccharides,<sup>12,13</sup> thereby leading to branched structures. Furthermore, it is not uncommon to find it as the terminal residue in an LPS<sup>14</sup> thereby being responsible for some of the cross-reactivities between different bacterial serogroups (which are defined by their respective O-antigen polysaccharides).

When an L-rhamnose residue is joined to another L-rhamnose sugar this often occurs as either an  $\alpha$ -(1  $\rightarrow$  2)- or  $\alpha$ -(1  $\rightarrow$  3)-linkage. Oligosaccharides having these structural elements have been investigated in detail by different research groups<sup>15–18</sup> and conformational descriptions with major and minor states have resulted from these studies. The dynamics of

<sup>a</sup> Department of Organic Chemistry, Arrhenius Laboratory, Stockholm University, S-106 91 Stockholm, Sweden. E-mail: [goran.widmalm@su.se](mailto:goran.widmalm@su.se)

<sup>b</sup> Dipartimento di Scienze Chimiche, Università degli Studi di Padova, Padova 35131, Italy. E-mail: [antonino.polimeno@unipd.it](mailto:antonino.polimeno@unipd.it)



L-rhamnose-containing oligosaccharides have also been examined employing  $^{13}\text{C}$  NMR spin relaxation studies,<sup>19</sup> analyzed by the model-free approach.<sup>20</sup> Another parameter utilized to obtain detailed information on conformational preferences is heteronuclear three-bond coupling constants,  $^3J_{\text{CH}}$ , but also homonuclear  $^3J_{\text{CC}}$ , readily available using site-specifically  $^{13}\text{C}$ -labeled compounds, are likewise very useful when interpreted *via* Karplus-type relationships.<sup>21</sup> Furthermore, the interpretation of different NMR observables is often aided by molecular dynamics (MD) simulations, from which a number of parameters can be calculated and compared to the experimentally measured ones.<sup>22,23</sup>

The disaccharide  $\alpha\text{-L-Rhap-}\alpha\text{-(1} \rightarrow 2\text{)-}\alpha\text{-L-Rhap-OMe}$  (R2R), the  $[1'\text{-}^{13}\text{C}]$ -isotopologue<sup>24</sup> of which is shown in Fig. 1, is a model for one of the commonly observed structural elements described above. In a previous  $^{13}\text{C}$  NMR spin relaxation study of four different disaccharides<sup>25</sup> it was observed that when DMSO- $d_6$ , in contrast to  $\text{D}_2\text{O}$ , is used as solvent, the correlation time ( $\tau_c$ ) of the molecule becomes such that measurements of the  $^{13}\text{C}\{^1\text{H}\}$  nuclear Overhauser effect outside the extreme narrowing regime are possible. Also, the NOE factor ( $1 + \eta$ ) is  $< 2.99$  and magnetic field dependent, ranging from  $\sim 2.8$  at 7.0 T to  $\sim 2.1$  at 14.1 T for the four disaccharides studied, but  $> 1.15$  (*i.e.*, the limit for slowly reorienting molecules). It should be noted that  $\tau_c$  was dependent on the number of hydroxyl groups in each disaccharide, *i.e.*, the higher the number of HO-groups interacting *via* hydrogen bonding to DMSO as an acceptor, the longer the correlation time. We have previously been able to show that  $^{13}\text{C}$  NMR spin relaxation data are reproduced by a combination of MD simulations and a stochastic approach, the diffusive chain model (DCM).<sup>26–28</sup> In this model the global reorientation dynamics of the molecule is considered in conjunction with the dynamics of the flexible molecule which was represented by rigid units connected by joints, where significant torsional motions were possible. Herein we describe the conformational preferences of  $\alpha\text{-L-Rhap-}\alpha\text{-(1} \rightarrow 2\text{)-}\alpha\text{-L-Rhap-OMe}$  (R2R) in water and dimethyl sulfoxide (DMSO) solutions based on MD simulations in the respective solvents, supported by transglycosidic  $^3J_{\text{CH}}$  and  $^3J_{\text{CC}}$  coupling constants. The  $^{13}\text{C}$  NMR spin relaxation data of  $[1'\text{-}^{13}\text{C}]$ -R2R in DMSO- $d_6$  at two magnetic fields are subsequently reproduced using the DCM in which the

relevant degree of freedom, *i.e.*, the  $\psi$  torsional angle is treated as the pertinent variable.

Stochastic approaches, when properly validated, can be a fast and accurate way to simulate and gather significant insight from NMR relaxation data. The stochastic model employed here for the interpretation of NMR observables is based on the choice of a set of relevant (slow) coordinates of the R2R molecule. This suggests that a *a posteriori* validation is desirable. We have compared results, *i.e.*, relaxation times and NOE, obtained from the model, which exhibit excellent agreement of calculated (without fitting parameters) and experimental NMR relaxation data, with a direct evaluation of the same observables obtained from MD simulations. The latter is nowadays an approach of choice, whenever long enough trajectories are available, which is not often the case for larger molecular systems. In this case, since R2R saccharide is a relatively small molecule, it is possible to access NMR relaxation times (agreeing to  $\sim 10\%$  error to experimental ones) directly from the MD simulations.

Finally, we have investigated the role of the coupling between the internal motion (*i.e.*, rotation about  $\psi$ ) and the global tumbling of the molecule. As discussed in the following, we show that the slow dynamics of the system arises from a strong interplay between these two degrees of freedom, suggesting that separation of time of scales between internal and global motions is not always valid and should be invoked with care.

## Theory

An integrated approach to describe flexible linear saccharides, previously introduced<sup>28</sup> (diffusive chain model, DCM) is employed. The computational treatment is based on (i) molecular dynamics simulations to evaluate the potential of mean force acting on internal soft torsion angles, (ii) a hydrodynamics approach to estimate the dissipative forces (diffusion tensor) acting on both the molecular global tumbling and the torsional dynamics, and (iii) a multidimensional diffusive equation to describe the joint internal and global dynamics.

The stochastic process associated with the relevant dynamics of R2R is represented by the general set  $\mathbf{Q} = (\boldsymbol{\Omega}, \boldsymbol{\theta})$ , where  $\boldsymbol{\Omega}$  is the set of Euler angles transforming from the laboratory frame (LF) to a molecule-fixed frame (MF), *cf.* Fig. 1, and  $\boldsymbol{\theta} = (\phi, \psi)$  describes all the torsion angles included explicitly in the (supposedly Markovian) set  $\mathbf{Q}$ .<sup>28</sup> Assuming that a diffusive Fokker-Planck description is acceptable, one can write the following time evolution equation for the conditional probability  $P(\mathbf{Q}, t | \mathbf{Q}_0, t_0)$  of the system<sup>29</sup>

$$\frac{\partial}{\partial t} P(\mathbf{Q}, t | \mathbf{Q}_0, t_0) = -\hat{\Gamma}(\mathbf{Q}) P(\mathbf{Q}, t | \mathbf{Q}_0, t_0)$$

$$\hat{\Gamma}(\mathbf{Q}) = - \left( \frac{\hat{\mathbf{M}}}{\partial \boldsymbol{\theta}} \right)^{\text{tr}} \begin{bmatrix} \mathbf{D}_{\text{RR}}(\boldsymbol{\theta}) & \mathbf{D}_{\text{RI}}(\boldsymbol{\theta}) \\ \mathbf{D}_{\text{RI}}^{\text{tr}}(\boldsymbol{\theta}) & \mathbf{D}_{\text{II}}(\boldsymbol{\theta}) \end{bmatrix} \quad (1)$$

$$\times P_{\text{eq}}(\mathbf{Q}) \left( \hat{\mathbf{M}} \frac{\partial}{\partial \boldsymbol{\theta}} \right) P_{\text{eq}}^{-1}(\mathbf{Q})$$

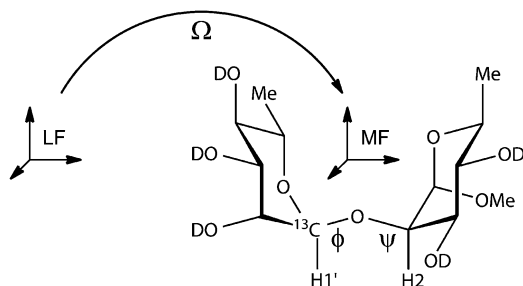


Fig. 1 Schematic of  $\alpha\text{-L-Rhap-}\alpha\text{-(1} \rightarrow 2\text{)-}\alpha\text{-L-Rhap-OMe}$  ( $[1'\text{-}^{13}\text{C}]$ -R2R). The glycosidic torsion angles  $\phi = \text{H1}'\text{-C1}'\text{-O2-C2}$  and  $\psi = \text{C1}'\text{-O2-C2-H2}$  are indicated and the transformation from the laboratory frame to the molecular frame fixed on the body bearing the spin probe, which diagonalizes the rotational part of the diffusion tensor of the molecule, is indicated by  $\boldsymbol{\Omega}$ .



where  $\hat{\mathbf{M}} = \hat{\mathbf{M}}(\Omega)$  is the infinitesimal rotation operator, the dissipative properties of the system are described by the diffusion tensor,  $\mathbf{D}(\theta)$ , partitioned in rotational, internal and internal-rotational blocks, while the equilibrium distribution is  $P_{\text{eq}}(\mathbf{Q}) = \exp[-V(\mathbf{Q})/k_{\text{B}}T] / \langle \exp[-V(\mathbf{Q})/k_{\text{B}}T] \rangle$ , where  $T$  is the temperature, and  $V(\mathbf{Q})$  the potential of mean force (POMF) acting on the system. All the operators and tensors are referred to a molecule-fixed frame and the diffusion tensor may, in general, depend upon molecular conformation.

To proceed, we need to evaluate the diffusion tensor and the POMF. The diffusion tensor is obtained by a hydrodynamic approach, which considers the molecule as a flexible set of linked spheres. Details of the procedure are described elsewhere.<sup>30</sup> Parameters entering the calculation are (i) the molecular geometry and (ii) the translational friction coefficient of a single sphere, given by Stokes's equation  $\xi = CR\pi\eta$ , as a function of the temperature-dependent bulk viscosity  $\eta$ , the effective radius of the spheres  $R$  and a constant  $C$  depending on the assumed boundary conditions.

In an isotropic medium, the POMF does not depend on the global orientation of the molecule. Therefore the equilibrium distribution depends only on the internal conformation, *i.e.*  $P_{\text{eq}}(\mathbf{Q}) = P_{\text{eq}}(\theta)/8\pi^2$ . An estimate of  $P_{\text{eq}}(\theta)$  can be provided by unbiased or biased MD simulations, depending on the complexity of the system under study. Eqn (1) can be solved numerically using linear algebra methods employing a representation with a proper basis set spanning the vector space of functions defined in  $\mathbf{Q}$ .<sup>31,32</sup> NMR relaxation data are evaluated directly, in the Redfield limit, from second rank correlation functions. Explicit expressions for the calculation of  $T_1$ ,  $T_2$ , NOE are given elsewhere.<sup>28,33</sup> The whole procedure is implemented in the C<sup>++</sup>OPPS software package<sup>34</sup> available for download under the GPL v2 license at the URL <http://www.chimica.unipd.it/licc/software.html>.

## Material and methods

### General

The atoms in the terminal rhamnosyl residue are denoted by a prime whereas those in the sugar residue linked to the *O*-methyl group are non-primed. The glycosidic torsion angles between the two sugar residues are defined as follows:

$$\phi = \text{H1}'\text{-C1}'\text{-O2-C2} \text{ and } \psi = \text{C1}'\text{-O2-C2-H2}.$$

### NMR spectroscopy experiments

All NMR experiments were recorded at 298.2 K where the temperature had been calibrated by a methanol-*d*<sub>4</sub> sample<sup>35</sup> prior to the start the experiments and processing of the acquired data was carried out using TopSpin 3 (Bruker). <sup>1</sup>H and <sup>13</sup>C NMR chemical shifts were referenced internally to DMSO-*d*<sub>5</sub> ( $\delta_{\text{H}}$  2.50) and DMSO-*d*<sub>6</sub> ( $\delta_{\text{C}}$  39.52), respectively.

An NMR sample of [1'-<sup>13</sup>C]-R2R<sup>24</sup> was prepared by freeze-drying from D<sub>2</sub>O and dissolving it in DMSO-*d*<sub>6</sub> (6.4 mg in 0.5 mL, 26 mM). The translational diffusion coefficient was measured using <sup>1</sup>H pulsed-field-gradient (PFG) spin-echo

experiments on a Bruker AVANCE III 600 MHz spectrometer (14.09 T) equipped with a 5 mm inverse Z-gradient TXI (<sup>1</sup>H/<sup>13</sup>C/<sup>31</sup>P) probe. In each experiment the PFG strength was increased linearly 32 times between 2% and 95% (100% = 55.7 G cm<sup>-1</sup>), with a PFG duration ( $\delta$ ) of 4 ms and a diffusion time ( $\Delta$ ) of 100 ms. The spectra were recorded with 32 scans using 16k data points for the acquisition, a spectral width of 14 ppm and an inter-scan delay of 5 s. The free induction decays (FIDs) were zero-filled twice and a 5 Hz exponential line broadening function was applied prior Fourier transformation. Translational diffusion coefficients were calculated using a protocol developed by Damberg *et al.*<sup>36</sup> The PFG calibration was performed using a doped water sample (1% H<sub>2</sub>O in D<sub>2</sub>O + 1 mg mL<sup>-1</sup> GdCl<sub>3</sub>) and a literature value of  $D_{\text{t}} = 1.90 \times 10^{-9} \text{ m}^2 \text{ s}^{-1}$  for the HDO resonance.<sup>37</sup> The diffusion coefficients of [1'-<sup>13</sup>C]-R2R and DMSO-*d*<sub>5</sub> were fitted to the integral decay of the resonances of the sugar bulk region (3.0–4.0 ppm) and to the solvent signal, respectively, and averaged values were calculated from nine independent measurements.

The <sup>13</sup>C NMR relaxation experiments were performed on a Bruker AVANCE III 700 MHz spectrometer (16.44 T) equipped with a 5 mm TCI Z-Gradient Cryoprobe and a Bruker AVANCE III 600 MHz spectrometer (14.09 T) equipped with a 5 mm BBO probe. The experiments were recorded with the carrier set in the region (100–102 ppm) near the <sup>13</sup>C-labeled anomeric resonance of [1'-<sup>13</sup>C]-R2R and with inter-scan delays of  $\geq 5$  s. Longitudinal relaxation times ( $T_1$ ) were measured with the fast inversion recovery experiment<sup>38</sup> using 14 different relaxation time delays ranging between 0.01 and 4 s in a shuffled manner for each experiment. Spectra were recorded with either 32 or 16 scans, 8k or 16k data points and spectral widths of 70 or 190 ppm, at 14.09 T and at 16.44 T, respectively. An exponential window function of 3 Hz was applied prior Fourier transformation whereupon peak intensities were extracted. The relaxation times were then fitted based on the peak intensities using an in-house MATLAB (MathWorks, R2012a) script and average values were calculated from 17 and 24 independent experiments, at the lower and higher magnetic field strengths, respectively. Transverse relaxation times ( $T_2$ ) were measured using a Carr-Purcell-Meiboom-Gill (CPMG) pulse sequence.<sup>39</sup> The delays between <sup>13</sup>C refocusing pulses in the pulse trains were set to 0.25 or 0.50 ms and the total length of the pulse-train was varied ten times in a shuffled manner for each experiment with a total pulse-train length from 5 to 300 ms. Spectra were recorded with 16 scans, using either 16k or 32k data points, and spectral widths of 100 or 120 ppm; an exponential window function of 5 Hz was applied prior Fourier transformation. The  $T_2$  relaxation times were then calculated from 20 and 15 independent experiments, respectively, using the TopSpin software. The NOE enhancement was calculated from the anomeric intensity ratio of a steady state NOE experiment with one long <sup>1</sup>H radiation time (5 s) and a short one (1 ms). Spectra were recorded with either 64 or 32 scans, 8k or 16k data points and spectral widths of 70 or 190 ppm; an exponential window function of 3 Hz was applied prior to Fourier transformation. Average NOE enhancement values were calculated from 18 and



24 experiments, respectively. The standard deviations for all the NMR relaxation data were  $\leq 1\%$ .

The  $^3J_{C1',H2}$  coupling constant was measured from the H2 multiplet ( $\delta_H$  3.65) in a 1D  $^1H$  NMR experiment, using the  $J$  doubling methodology<sup>40,41</sup> implemented in-house by a MATLAB script. The spectrum was recorded on the 700 MHz NMR spectrometer with 64 scans and an acquisition time of 2.3 s. Resolution enhancement was achieved by applying a Gaussian window function centered at 0.9 s in the FID together with an lb =  $-2$  Hz. The  $^3J_{C1',C1}$  and  $^3J_{C1',C3}$  coupling constants were measured employing the  $J$  doubling methodology to the peak-to-peak separation of the C1 resonance ( $\delta_C$  99.90) and the C3 resonance ( $\delta_C$  70.43) in a  $^{13}C$  spectrum, recorded with 1k scans and an acquisition time of 4.0 s. Resolution enhancement was achieved by using a Gaussian window function centered at 1.2 s in the FID together with an lb =  $-2$  Hz.

Additional NMR measurements were carried out on a sample of  $[1'-^{13}C]$ -R2R in  $D_2O$  (30 mg mL $^{-1}$ )<sup>24</sup> at 14.09 T using a 5 mm BBO probe. The NOE experiments were recorded with 128 scans in addition to four dummy scans and with an inter-scan delay of 20 s. FIDs were acquired with 64k data points and were multiplied with an exponential window function of 3 Hz prior the Fourier transformation. The NOE enhancement was calculated as the intensity ratio of the anomeric resonance from C1' using an experiment with a long (2 s) and with a short (1 ms) mixing-time. An average NOE value was calculated from ten independent measurements. Translational diffusion measurements, using the BBO probe, were performed as described above.

### Molecular dynamics simulations

MD simulations were performed using the CHARMM program (v. 36b1)<sup>42</sup> based on the CHARMM additive all-atom carbohydrate force field.<sup>43</sup> Initial coordinates for the disaccharide were obtained from the topology information present in the force field. For the aqueous simulation, the CHARMM modified TIP3P parameters were used,<sup>44</sup> and for the simulation in DMSO, the Strader-Feller parameters were employed.<sup>45</sup> The disaccharide was placed in a pre-equilibrated solvent box containing either 900 waters or 230 DMSO molecules. Solvent molecules with any heavy atom closer than 2.6 Å to the solute were removed, leaving 881 and 223 for the aqueous and DMSO simulations, respectively. The potential energies of the systems were minimized using 1000 steps with the steepest descent method followed by 5000 steps using the adopted basis Newton-Raphson method. Velocities were assigned at 100 K and the system heated to 298.15 K during 10 ps, followed by equilibration during 500 ps. Leap-frog integration was performed using a time step of 2 fs until 100 ns had been sampled, saving coordinates every 2 ps. Pressure and temperature were maintained at 1 atm and 298.15 K using the Nosé-Hoover barostat and thermostat, respectively.<sup>46,47</sup> Bonds to hydrogen atoms were kept rigid using SHAKE.<sup>48</sup> Electrostatics were handled using the particle-mesh Ewald method,<sup>49</sup> and the other non-bonded interactions were smoothly switched off between 10 and 12 Å. The viscosity for the pure DMSO solvent was determined from a 15 ns simulation.

The elements of the pressure tensor were saved at every 2 fs step. The Green-Kubo method was used to obtain the viscosity from the off-axis elements of the pressure tensor. The translational self-diffusion coefficient was calculated from the slope of the mean-squared displacement function obtained for the complete simulation trajectory. The obtained value was corrected for the finite size of the box,<sup>50</sup> using the viscosity determined for the corresponding pure solvent. Spatial distribution functions were generated at 0.2 Å resolution in CHARMM and smoothened using a Gaussian function ( $\sigma = \sqrt{2}/5$ ) before interpolating to 0.1 Å resolution using the 'spline' option in Octave, version 3 (<http://www.gnu.org/>).<sup>51</sup> As the bulk solvent density, the median density was used. The resulting density matrix was visualized together with the molecule using PyMOL (The PyMOL Molecular Graphics System, Version 1.5.0.1 Schrödinger, LLC) (<http://www.pymol.org/>).

## Results and discussion

### Molecular dynamics simulations

In water as well as in DMSO solution, the  $\phi$  torsion angle in the R2R disaccharide adopts a single, *exo*-anomeric conformation, with  $\langle\phi\rangle = 42^\circ$  in water, and  $\langle\phi\rangle = 45^\circ$  in DMSO. In contrast, in both solvents the  $\psi$  torsion angle exhibits a conformational exchange between two different states as is evident from its bimodal distribution in Fig. 2. These two states, referred to as  $\psi^+$  and  $\psi^-$ , are characterized by being centered on positive and negative values of the  $\psi$  torsion angle, respectively (Table 1). The  $\psi^+$  and  $\psi^-$  conformational states are present in a 0.41 : 0.59 ratio in the water simulation, whereas in DMSO the equilibrium is shifted towards the  $\psi^+$  conformation, resulting in a 0.68 : 0.32 ratio. This solvent-induced change between the major conformations is illustrated in Fig. 3. Thus, the MD simulations indicate that solvent induces a conformational change from water as a solvent, where the major conformational state is

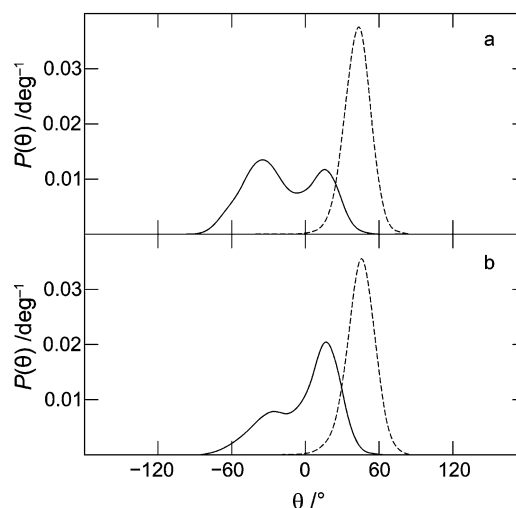


Fig. 2 Probability distribution functions of the glycosidic torsion angles in R2R from the MD simulations in (a) water and (b) DMSO;  $\phi$  (dashed line) and  $\psi$  (solid line).

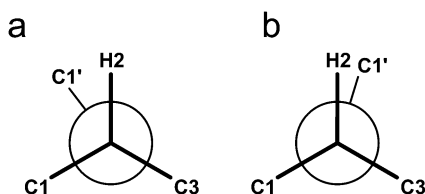




**Table 1** Averages from the  $^3J$ -based analysis and MD simulations for R2R in water and DMSO together with experimental  $^3J_{CH}$  and  $^3J_{CC}$  NMR coupling constants

	Water				DMSO			
	Expt <sup>a</sup>	MD	$\psi^+$ (MD)	$\psi^-$ (MD)	Expt	MD	$\psi^+$ (MD)	$\psi^-$ (MD)
Population MD			0.412	0.588			0.680	0.320
$\phi/^\circ$		42.1 (11) <sup>b</sup>	45.4 (12)	39.9 (10)		44.8 (12)	46.4 (12)	41.4 (12)
$\psi/^\circ$		-16.9 (29)	13.3 (13)	-38.1 (16)		-0.1 (26)	15.4 (13)	-33.1 (15)
$^3J_{H1',C2}/\text{Hz}$	4.2	4.07	3.77	4.28	4.0 <sup>g</sup>	3.81	3.66	4.10
$^3J_{C1',H2}/\text{Hz}$	4.6	4.58	5.66	3.83	5.04	5.16	5.57	4.29
$^3J_{C1',C1}/\text{Hz}$	0.70	1.48	2.36	0.86	0.96	1.95	2.49	0.79
$^3J_{C1',C3}/\text{Hz}$	1.90	2.07	0.42	3.23	0.99	1.17	0.33	2.96
Population $\langle^3J\rangle^h$			0.36	0.64			0.56	0.44

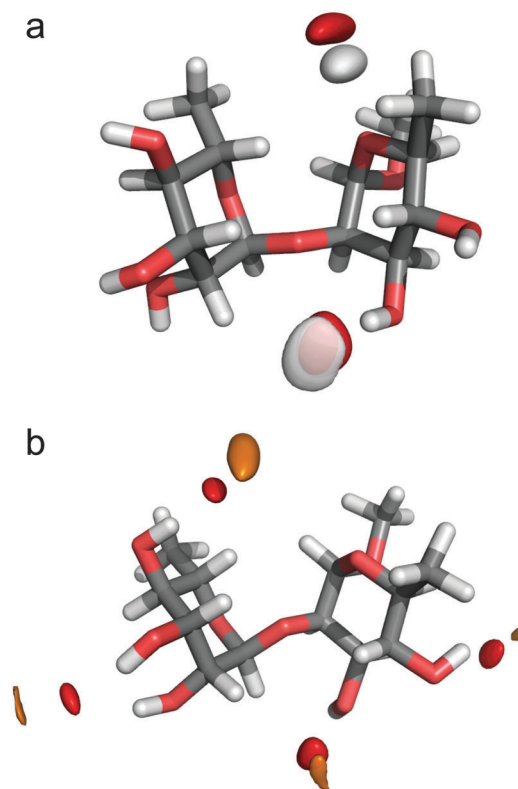
<sup>a</sup> Heteronuclear coupling constants are averages from different methods for their measurements according to Jonsson *et al.*<sup>24</sup> <sup>b</sup> Root-mean-square deviations are given in parenthesis. <sup>c</sup> Calculated using eqn (9) from S       *et al.*<sup>59</sup> <sup>d</sup> Calculated using eqn (10). <sup>e</sup> Calculated using eqn (8), with a constant-in-plane (CIP) addition.<sup>59</sup> <sup>f</sup> Calculated using eqn (8), without CIP effect. <sup>g</sup> Hardy *et al.*<sup>60</sup> <sup>h</sup> Populations derived using  $\langle^3J_{C1',H2}\rangle$ ,  $\langle^3J_{C1',C1}\rangle$  and  $\langle^3J_{C1',C3}\rangle$  in the  $\psi^+$  and  $\psi^-$  states from the MD simulations.

**Fig. 3** Newman projections of the  $\psi$  torsion angle showing the major conformational state (a) in water having  $\langle\psi\rangle = -38^\circ$  and (b) in dimethyl sulfoxide (DMSO) having  $\langle\psi\rangle = 15^\circ$ .

known to have the  $\psi^-$  conformation,<sup>18</sup> to a  $\psi^+$  conformation as the major one. Transglycosidic NMR  $J$  coupling constants were then calculated from the two MD simulations and revealed differences for both hetero- and homonuclear  $J$  values between the solvents as well as between the conformational states populated (Table 1).

From the MD simulation translational diffusion coefficients and DMSO solvent viscosity were also calculated. The disaccharide had  $D_t^{298} = 2.16 \times 10^{-10} \text{ m}^2 \text{ s}^{-1}$  whereas DMSO showed  $D_t^{298} = 7.24 \times 10^{-10} \text{ m}^2 \text{ s}^{-1}$  for a box of pure solvent. Additionally, the shear viscosity of the solvent was calculated as  $\eta^{298} = 2.32 \text{ cP}$ , closely similar to that of DMSO- $d_6$ ,  $\eta^{298} = 2.19 \text{ cP}$ <sup>52</sup> which was the solvent used for the NMR spin relaxation experiments. Thus, as the viscosity derived from the MD simulation agrees very well with that of the solvent used experimentally, the MD simulations should be suitable for calculation of NMR observables.

Spatial distribution functions (SDFs)<sup>53–55</sup> were used to investigate the solvent structure around the disaccharide. For the major conformation of R2R in water and in DMSO regions with higher solvent density than the bulk were possible to identify. In water solution two conspicuous regions were evident, *viz.*, (i) a water molecule acting as a hydrogen bond acceptor to the HO3 hydroxyl group of the rhamnosyl residue carrying the O-methyl group and (ii) a water molecule donating a hydrogen bond to the ring oxygen of the same sugar residue (Fig. 4a). It can be noted that for the R2R molecule inter-residual hydrogen bonding is not present, in contrast to *e.g.* the disaccharides cellobiose<sup>56</sup> or sucrose;<sup>57</sup> thus, its conformational preferences at the glycosidic linkage are indeed governed also by solvent

**Fig. 4** Spatial distribution functions (SDFs) calculated for the major conformation of R2R in water (a) and in DMSO (b); surfaces enclosing regions with a density 7.3 and 3.6 times the bulk density for water oxygen (red) and hydrogen (white), respectively, and a density of 18 and 9.0 times the bulk density for DMSO oxygen (red) and sulfur (yellow), respectively.

cage interactions. In DMSO solution the hydroxyl groups of R2R are involved in hydrogen bonding to the oxygen atoms of the solvent acting as acceptors (Fig. 4b).

### NMR spectroscopy and spin relaxation

The coupling constants across the glycosidic linkage can be measured accurately<sup>58–60</sup> and changes in these quantities, which depend on environmental alterations such as stereochemistry, temperature or solvent, can be monitored readily. Related to the



$\phi$  torsion angle the  $^3J_{\text{H1}',\text{C2}}$  values are quite similar and of the same magnitude between the two solvents (Table 1). This is also the case for the  $^3J_{\text{C1}',\text{C1}}$  values related to the  $\psi$  torsion angle, but in contrast to the  $^3J_{\text{H1}',\text{C2}}$  coupling the computed values from the MD simulations for  $^3J_{\text{C1}',\text{C1}}$  do not agree to the same extent which may call for a revision of the Karplus-type relationship for this geometrical arrangement of the  $^3J_{\text{CC}}$  coupling across the glycosidic linkage. However, with respect to the latter torsion angle both  $^3J_{\text{C1}',\text{H2}}$  and  $^3J_{\text{C1}',\text{C3}}$  differ notably and sufficiently to conclude that a conformational change takes place between the two solvents. By using the three available  $^3J_{\text{C1}',\text{X}}$  coupling constants, where X refers to H or C, together with the corresponding calculated values in each of the two conformational states and optimizing the relative populations of the two states, it is shown experimentally that the  $\psi^+$  and  $\psi^-$  conformational states are present in a 0.36:0.64 ratio in water, while in DMSO the equilibrium favors the  $\psi^+$  conformation, in a 0.56:0.44 ratio; in both cases similar to the proposed equilibria from the MD simulations (*vide supra*).

Different NMR relaxation data are often measured at more than one magnetic field strength in order to obtain a sufficiently large number of observables to fit to motional parameters of dynamic models.<sup>61,62</sup> For small molecules in low viscosity solvents the rotational reorientation is rapid and the NMR relaxation parameters are independent of the magnetic field employed, *i.e.*, the extreme narrowing region prevails where  $\omega^2\tau_c^2 \ll 1$ .<sup>63</sup> For a sample of  $[1'-^{13}\text{C}]\text{-R2R}$  in  $\text{D}_2\text{O}$  at 298 K the heteronuclear NOE factor at 14.1 T was determined herein revealing NOE = 2.70, *i.e.*, quite close to the theoretical maximum of the NOE factor, where it will be difficult to extract reliable information about internal motion from such data.<sup>64</sup> For the translational diffusion measurements,  $D_t^{298} = 4.59 \times 10^{-10} \text{ m}^2 \text{ s}^{-1}$ , the molecular global correlation time was deduced,  $\tau_c = 90 \text{ ps}$ , consistent with that determined at 310 K, *viz.*,  $\tau_c \approx 65 \text{ ps}$ .<sup>65</sup> In order to utilize the magnetic field dependence of, in particular, the heteronuclear NOE<sup>66</sup> for the molecule under study, it was decided that DMSO- $d_6$  would be the solvent of choice (*cf.* ref. 25 where the suitability of the solvent in conjunction with available magnetic field strengths for disaccharides had been established).  $^{13}\text{C}$  NMR spin-lattice relaxation times  $T_1$ , spin-spin relaxation times  $T_2$ , and heteronuclear NOE factors ( $1 + \eta$ ) were thus measured for R2R in DMSO- $d_6$  at two magnetic field strengths, *viz.*, 14.1 T and 16.4 T, and these are given in Table 2. Notably, due to the very high  $^{13}\text{C}$ -labeling of 99 atom% at the C1'-position<sup>24</sup> the quality of the data was very high and the standard deviations for all the NMR relaxation data was  $\leq 1\%$ . Translational diffusion was

also determined for the disaccharide which had  $D_t^{298} = 2.83 \times 10^{-10} \text{ m}^2 \text{ s}^{-1}$  whereas DMSO- $d_6$  in the same sample showed  $D_t^{298} = 5.28 \times 10^{-10} \text{ m}^2 \text{ s}^{-1}$ , confirming that the MD simulations gave reasonable results also for these physical properties.

### Stochastic modeling of NMR relaxation data

For R2R in DMSO- $d_6$  at 298.15 K NMR relaxation data were simulated using the DCM by including only one torsional degree of freedom. To this purpose, the MD trajectory was analyzed, evaluating initially a two dimensional POMF in the torsion angles ( $\phi, \psi$ ). Since a sharp population maximum around  $46.4^\circ$  was observed for  $\phi$  (*cf.* Fig. 2) we neglected the dependence on this torsion angle and kept  $\psi$  as the only relevant internal degree of freedom. The one-dimensional POMF, shown in Fig. 5, was obtained

after interpolation as a Fourier series  $\frac{U(\psi)}{k_B T} = \sum_{n=-N}^N \varepsilon_n \exp(in\psi)$  with coefficient  $\varepsilon_{-n} = \varepsilon_n^*$  listed in Table 3 up to  $n = 12$ . Finally the rotational + internal  $4 \times 4$  diffusion tensor of R2R, was calculated with a viscosity for DMSO- $d_6$  of 2.19 cP, a sphere radius 2.0 Å and stick boundary conditions. Following previous work, constant values of the diffusion tensor elements were chosen corresponding to the value of  $\psi$  in the minimum of the POMF. The principal axes of rotation with respect to the diagonalized rotational block  $\bar{\mathbf{D}}_{\text{RR}}$  were defined, thus choosing a molecular frame (MF) so that the final form of the (approximated) diffusion tensor is

$$\bar{\mathbf{D}} = \begin{pmatrix} \bar{\mathbf{D}}_{\text{RR}} & \bar{\mathbf{D}}_{\text{RI}} \\ \bar{\mathbf{D}}_{\text{RI}}^{\text{tr}} & \bar{\mathbf{D}}_{\text{II}} \end{pmatrix} \approx \begin{pmatrix} 6.41 \times 10^8 & 0 & 0 & -7.73 \times 10^7 \\ 0 & 6.41 \times 10^8 & 0 & -1.81 \times 10^8 \\ 0 & 0 & 1.68 \times 10^8 & -1.51 \times 10^9 \\ -7.73 \times 10^7 & -1.81 \times 10^8 & -1.51 \times 10^9 & 2.73 \times 10^9 \end{pmatrix} \text{ Hz} \quad (2)$$

here the rotational part of the diffusion tensor is approximated to an axially symmetric form by averaging the original  $D_{\text{XX}} = 6.00 \times 10^8 \text{ Hz}$  and  $D_{\text{YY}} = 6.82 \times 10^8 \text{ Hz}$  components. Although not strictly necessary – since the  $\text{C}^{++}\text{OPPS}$  program can handle a fully anisotropic diffusion tensor – this approximation simplifies, without appreciable differences in the results, the discussion on the coupling between internal and global motions (see the next subsection). An adimensional scaling parameter<sup>28</sup> was introduced in the past as an adjustable number to take into

**Table 2** Comparison among experimental, exact stochastic model, molecular dynamics, and decoupled stochastic model NMR relaxation data for the disaccharide R2R in DMSO- $d_6$  at 298.2 K

	$^1\text{H}$ frequency/MHz	Experimental	DCM exact	DCM exact  err /%	MD	MD  err  %	DCM decoupled	DCM decoupled  err  %
$T_1/\text{ms}$	600.1	440.0	429.5	2.4	487.1	10.7	316.4	28.0
$T_2/\text{ms}$		402.6	396.0	1.6	452.4	12.4	302.2	24.9
NOE		2.361	2.314	2.0	2.381	0.85	2.620	11.0
$T_1/\text{ms}$	700.0	475.6	469.5	1.3	525.1	10.4	335.7	29.4
$T_2/\text{ms}$		432.9	426.4	1.5	481.8	11.3	317.5	26.7
NOE		2.215	2.188	1.2	2.290	3.4	2.536	14.5



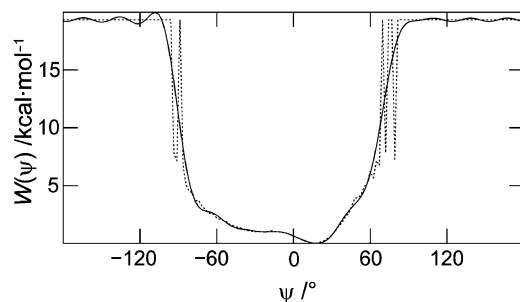


Fig. 5 Potential of mean force (POMF) of the glycosidic torsion angle  $\psi$  from the MD simulation using DMSO as solvent (dotted line) and the one obtained after interpolation as a Fourier series and used in the simulation of  $^{13}\text{C}$  NMR relaxation data (solid line).

Table 3 Fourier coefficients for the potential of mean force related to the  $\psi$  torsion angle

$n$	$\text{Re } \epsilon_n$	$\text{Im } \epsilon_n$
0	11.6	0
1	5.51	0.842
2	1.21	0.362
3	-1.03	0.598
4	-0.542	0.557
5	0.335	-0.192
6	0.205	-0.356
7	-0.185	0.132
8	-0.11	0.310
9	0.0628	-0.0211
10	0.0089	-0.204
11	-0.0568	0.0297
12	0.0501	0.0948

account the uncertainty of the model due to the effective radius and boundary conditions. However, here we avoided *on purpose* any further refinement, so that we can assess directly how the model and the direct MD simulations compare. Other relevant geometrical parameters are: (i) the Euler angle transforming the MF into the principal axis of the dipolar tensor (DF)  $\Omega_{\text{MF} \rightarrow \text{DF}} = (0^\circ, 60.8^\circ, -10.4^\circ)$  and (ii) the distance  $r_{\text{CH}} = 1.13 \text{ \AA}$ , which accounts for bond vibrations.<sup>67,68</sup>

The comparison of experimental NMR data with calculations performed with C<sup>++</sup>OPPS is presented Table 2. The program implements the solution of a Smoluchowski equation by projecting the diffusive operator on a set of orthonormal basis functions  $|LMKn\rangle = \sqrt{(2L+1)D_{\text{MK}}^J(\Omega)} \exp(in\psi)/4\pi\sqrt{\pi}$ , followed by direct tridiagonalization of the resulting symmetric matrix *via* Lanczos algorithm.<sup>28,31</sup> Matrices with dimensions of the order of  $10^3$  need to be treated.<sup>28</sup> The numerical simulation shows excellent agreements with the relaxation parameters at the two frequencies of 600.132 and 699.973 MHz (Table 2).

### Coupling between internal and global dynamics

In this subsection, we investigate if, and to which extent, the coupling between global and internal motions in the R2R molecule is relevant with respect to NMR relaxation.

As was sketched in the Introduction, we employ the MD trajectory as a further way of validation of the model. To this purpose, we first test the validity of the MD simulation itself by calculating

R2R NMR relaxation data. The R2R trajectory is referred to a reference frame, CF, centered on the center of mass of the molecule, and arbitrarily oriented over the molecule. Then, we extract the time series of the orientation of the  $^{13}\text{C}-^1\text{H}$  bond,  $\Omega(t)$ , with respect to CF, and we calculate the Wigner matrix element  $D_{0,0}^2(\Omega(t))$  function, which, in the secular approximation, is the only function used to define the dipolar-dipolar spectral density. In particular, given the time series of the Wigner matrix, we calculate the (normalized) autocorrelation function  $C(t) = 5\langle D_{0,0}^2(\Omega(t))D_{0,0}^2(\Omega(0)) \rangle$ . Finally, the spectral density for the  $^{13}\text{C}-^1\text{H}$  dipolar interaction is calculated as the Fourier-Laplace transform of  $C(t)$ . We stress here that in order to obtain a reasonable spectral density from the MD trajectory, the correlation function must firmly be at convergence since, among other information, the spectral density at zero frequency is required (which, in turn, requires that the long-time behavior of the autocorrelation function is calculated correctly). It is worthy to note that, despite of the apparent ‘simplicity’ of the system, a 100 ns long trajectory is barely enough for calculating a good correlation function. In practice, we split the trajectory into two trajectories of 50 ns each, which facilitated fitting of the correlation function to a bi-exponential decay. Autocorrelation functions are calculated for each of the two sub-trajectories, and then summed and renormalized. The resulting function is fitted with a bi-exponential functional form:  $C(t) = ae^{-\omega_a t} + be^{-\omega_b t}$ . Best fitting parameters are:  $a = 0.471$ ,  $\omega_a = 3.687 \times 10^9 \text{ Hz}$ ,  $b = 0.529$ , and  $\omega_b = 1.456 \times 10^{10} \text{ Hz}$ . The spectral density is analytic and NMR data are easily accessed. Table 2 shows the results, obtained with a CH bond length of 1.111 Å (*i.e.*, the value of the bond length in the MD force field, without the need of vibrational correction). The agreement with experiment is satisfactory, all data reproduced with an error of  $\sim 10\%$  or less.

From the MD simulations the  $T_1$  and  $T_2$  relaxation times and the NOE values are consistently longer and higher, respectively, than what are observed from experiments (Table 1). Thus, the correlation time  $\tau_c$  from the MD simulation is shorter than from experiment, despite the fact that the shear viscosity of the solvent calculated from the MD simulation was slightly higher than that determined experimentally for DMSO- $d_6$  as solvent (*vide infra*). This deviation in  $\tau_c$  may be due to the fact that the potential describing the solute-solvent interaction is somewhat weaker than needed for a correct description of the rotational correlation time, *i.e.*, its part in the ‘interaction triad’ would have to be optimized further.<sup>69</sup>

We also investigate the role of coupling between internal conformational motions and global tumbling. In our stochastic model, the global and internal motions are rigorously treated as coupled. We can easily explore what happens in absence of coupling between internal and global motions. In the DCM, the molecule is partitioned in two rigid fragments, which can rotate with respect to each other around the selected bond ( $\psi$  dihedral angle). When global tumbling is considered to be uncoupled from the torsional angle  $\psi$ , the decoupled correlation function reads

$$C_d(t) = \frac{1}{5} \sum_{k=-2}^2 e^{-\omega_k t} c_k(t) \quad (3)$$



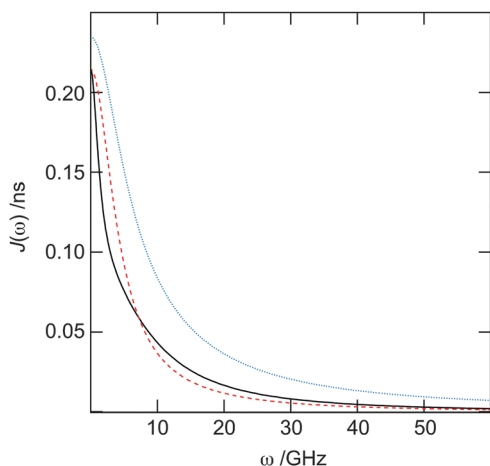


Fig. 6 Dipolar–dipolar spectral densities for the  $^{13}\text{C}$ – $^1\text{H}$  probe obtained from  $D_{0,0}^2$  autocorrelation functions: MD (black, solid line), DCM exact (red, dashed line) and DCM decoupled (blue, dotted line).

where  $\omega_k = 6D_{\text{RR},\perp} + k^2(D_{\text{RR},\parallel} - D_{\text{RR},\perp})$ , and  $c_k(t) = \langle D_{k,0}^2(\Omega_i(t))^* \times D_{k,0}^2(\Omega_i(0)) \rangle$  are the ‘internal’ autocorrelation functions. Note that the decoupling of the motions does not always imply that the correlation function is factorized, but rather that it can be written as the sum of factorized products. Results are reported in Table 2. Calculated relaxation times exhibit a 20–30% error, compared with experiment, and NOEs – which are usually evaluated with higher accuracy – show relative errors of 10–15%. Clearly, the decoupled scheme provides an unacceptable comparison with experimental, MD and DCM exact data. Fig. 6 compares visually the spectral densities obtained from the three approaches, MD, DCM exact and DCM uncoupled. It is evident that decoupling internal and global motions leads to a serious overestimation of the effective correlation times.

### Comparison with other oligosaccharides

The stereochemistry and substitution pattern of carbohydrates facilitate many different arrangements on how oligosaccharides can be linked together, such as open (linear or branched) chains of sugar units as well as rings, *i.e.*, closed geometries.

NMR relaxation studies have been informative on the dynamics of several open-chain oligosaccharides built of two to five sugar units. Small, di- and trisaccharides, were extensively studied *via* MD simulations. Data on the flexibility at the glycosidic linkages can then be obtained through the calculation of mean-force potentials and correlation times. Information from MD can be merged with molecular rotational reorientation, deduced from experimental translational diffusion values, thus allowing the calculation of NMR relaxation data.<sup>55,70</sup>

In a recent study, an MD simulation was coupled to a model-free approach for the interpretation of  $^{13}\text{C}$  NMR  $T_1$  relaxation times of sucrose,<sup>64</sup> thus assuming decoupling between global and internal dynamics. The  $D_{0,0}^2$  time correlation function for each  $^{13}\text{C}$ – $^1\text{H}$  pair was fitted to a double-exponential. The same approach was previously used in a study of trisaccharide dynamics.<sup>70</sup> The calculated  $^{13}\text{C}$   $R_1$  and  $R_2$  relaxation rates of sucrose were slightly underestimated in pure water, whereas in

a water–DMSO mixture they were overestimated due to faster and slower reorientational dynamics, respectively. For these small saccharides, model-free analysis returned quite high ordering, that would suggest that the motion of the  $^{13}\text{C}$ – $^1\text{H}$  probe is confined in a quite narrow potential well. Also,  $\tau_m$  and  $\tau_e$  differed by just one order of magnitude. Comparing these conclusions to the disaccharide studied in this work (see Fig. 5), as well as the di- and tri-saccharides studied in ref. 26 and 28, respectively, an order parameter of 0.9 appears to be overestimated, since if one considers that thermal energy is about  $2.5 k_B T$  units at 298.15 K, the span at a  $\psi$  torsion likely covers a  $120^\circ$  range, while around a  $\phi$  torsion, a  $60^\circ$  range is expected. Also, values of the rotational and internal parts of the diffusion tensors for the molecules suggest that motions may occur on similar time scales, requiring an explicit modeling approach, such as the DCM, for the coupling between motions occurring on closely related time scales, which was found to be the case in small oligosaccharide dynamics.<sup>26,28</sup>

Similar arguments apply to larger saccharides composed of four or five sugar units. In the model-free analysis of the tetrasaccharide LNnT the two inner sugar residues showed more restricted motions, *i.e.*, the generalized order parameters  $S^2$  were higher and closer to unity than for the terminal sugar residue.<sup>71</sup> Similar results were also drawn from a study of a branched tetrasaccharide.<sup>72</sup> The trisaccharide melezitose in which a fructose residue is disubstituted by two glucosyl residues exhibited a larger  $S^2$  value for the fructose residue,<sup>73</sup> although it can be anticipated to show some pseudorotation for the 5-atom-membered furanose ring. However, like in LNnT the central residue exhibited the highest generalized order parameter. In a study of a mannosyl-containing pentasaccharide  $^{13}\text{C}$  NMR  $T_1$  relaxation times were measured and the MD simulation was utilized as the basis for comparison and evaluation of overall hydrodynamic behavior and internal motions.<sup>74</sup> From the MD trajectory, the spectral density function  $J(\omega)$  was calculated explicitly by Fourier transformation of the angular correlation function, and subsequently calculation of the  $T_1$  value from its dependence on the combination of spectral densities. It was concluded that, within experimental error, the computed  $T_1$  values based on the MD simulation were in agreement with the experimentally measured ones. In a pentasaccharide, being a model for part of *N*-glycan structures of glycoproteins, the disaccharide *N*-acetylglucosamine substituted positions 2 and 6 of a mannosyl residue, *i.e.*, for the latter one an additional degree of freedom exists; the flexibility for the disaccharide substituting O6 was higher, consistent with the fact that the  $\omega$  torsion angle (O5–C5–C6–O6) populates at least two conformational states.<sup>75</sup> Furthermore, the stereochemistry and the substitution patterns at the glycosidic linkage influence the dynamics, *e.g.*, in an  $\alpha$ -(1  $\rightarrow$  4)-linked fucosyl-containing disaccharide the flexibility was higher than in the  $\beta$ -(1  $\rightarrow$  4)-linked methyl  $\alpha$ -cellobioside,<sup>25</sup> which can either be due to the inherent difference between  $\alpha$ - and  $\beta$ -linked pyranosides or stemming from the presence of an intramolecular interresidual hydrogen bond stabilizing the molecular structure, thereby resulting in a more rigid disaccharide. Furthermore, the role of rotational anisotropy, in addition to flexibility, was thoroughly investigated





for the pentasaccharide LNF-1, in which a differential and larger flexibility was observed toward the reducing end of the oligosaccharide.<sup>76</sup> We described LNF-1 at the DCM level, using an initial MD simulation to identify the relevant degrees of freedom.<sup>28</sup> Of the eight glycosidic torsion angles those toward the terminal part of LNF-1 were identified as 'rigid' (in the sense of having faster relaxation relatively to the other torsions – see Section S2 of the ESI of ref. 28) whereas the other ones toward the reducing end of the molecule were considered flexible. Once the DCM with the 'proper' complexity had been deduced from MD simulations, Brownian dynamics simulations were adopted to obtain correlation functions, spectral densities and eventually <sup>13</sup>C NMR relaxation parameters. Notably, as in this work, no further refinement was needed in order to observe good agreement ( $\pm 10\%$ ) between simulated and experimental <sup>13</sup>C NMR parameters.

Finally, closed-chain geometries can be addressed. In particular, cyclodextrins have been studied<sup>27</sup> using both the model-free approach and a two-body general approach (Slowly Relaxing Local Structure, SRSLS).<sup>77</sup> In a model-free analysis of the  $\alpha$ - and  $\gamma$ -cyclodextrins that contain six and eight glucosyl residues, respectively, in a cyclic fashion, the flexibility was found being slightly larger (lower  $S^2$ ) in the latter compound,<sup>78</sup> presumably due to less strain in the cyclic molecule.

## Conclusions

The MD simulations of the disaccharide with explicit solvent molecules proposed different preferred conformational states for the  $\psi$  torsion angle between water and DMSO solutions, a finding that was confirmed by interpretation of experimentally determined transglycosidic NMR scalar couplings constants. The good agreement shown by simulated results obtained *via* the application of the DCM with the experimental values of relaxation times is a direct consequence of the assumption of a strong coupling between internal (conformational) and rigid-body (rotational) degrees of freedom for R2R. This is to be expected for relatively small and flexible molecular systems, in which the usual assumption of a complete lack of correlation between tumbling and conformational relaxation processes is incorrect. Thus, it is not really possible to interpret slow motion of the R2R molecule simply as a 'direct sum' of global and internal dynamics. Their coupling makes global tumbling affecting rotation about the  $\psi$  angle and *vice versa*. In such a scenario, the 'global plus internal' motion paradigm should be abandoned in favor of a more general view of structural fluctuation of the molecule, when dealing with the interpretation of physico-chemical processes directed by slow dynamics.

We stress that while it is true that MD simulations offer the possibility to include trivially all the relaxation processes occurring in a molecule, slow processes are still difficult to sample. The larger the molecule, the longer (in a non-linear way) is the simulation time required to gain sufficient statistics. Also, ergodicity is an important problem; standard thermostatic MD simulations are not assured to allow a complete exploration

of the phase space, no matter how long (realistically) the trajectory is protracted.

Conversely, a model approach can be efficiently employed. Validation can be based, for relatively small systems, on long enough MD trajectories. In this work, a 100 ns long trajectory of the R2R molecule was used and also employed to recover the mean force potential adopted in the stochastic model.

We have shown that the relevant dynamics of a 'short linear chain' of sugar rings can be safely described using a DCM model, where internal flexibility is given in terms of dihedral angles. Our results suggest that a protocol in which (i) short MD simulations are used on one hand to detect the most relevant dihedral angles, and on the other hand, to access the potential of mean force, and (ii) hydrodynamics modeling is employed for the friction, can provide a complete parametrization of a diffusive coupled approach accurate enough to reproduce long-time dynamics behavior of oligosaccharides.

## Acknowledgements

This work was supported by the Swedish Research Council, The Knut and Alice Wallenberg Foundation, and the Fondazione della Cassa di Risparmio di Padova e Rovigo, project M<sub>3</sub>PC. Computing resources were kindly provided by the Swedish National Super-computer Centre, Linköping University, and by the Computational Chemistry Community of the University of Padova.

## References

- 1 G. Widmalm, *Carbohydr. Res.*, 2013, **378**, 123–132.
- 2 R. Taufik, K. Fukuda, A. Senda, T. Saito, C. Williams, C. Tilden, R. Eisert, O. Oftedal and T. Urashima, *Glyco-conjugate J.*, 2012, **29**, 119–134.
- 3 F.-G. Hanisch, H. Ragge, T. Kalinski, F. Meyer, H. Kalbacher and W. Hoffmann, *Glycobiology*, 2013, **23**, 2–11.
- 4 M. Lahaye and A. Robic, *Biomacromolecules*, 2007, **8**, 1765–1774.
- 5 H.-J. Gabius, H.-C. Siebert, S. André, J. Jiménez-Barbero and H. Rüdiger, *ChemBioChem*, 2004, **5**, 740–764.
- 6 E. V. Vinogradov, B. O. Petersen, J. E. Thomas-Oates, J. Ø. Duus, H. Brade and O. Holst, *J. Biol. Chem.*, 1998, **273**, 28122–28131.
- 7 M. Linnerborg, G. Widmalm, A. Weintraub and M. J. Albert, *Eur. J. Biochem.*, 1995, **231**, 839–844.
- 8 M. Ansaruzzaman, M. J. Albert, T. Holme, P.-E. Jansson, M. M. Rahman and G. Widmalm, *Eur. J. Biochem.*, 1996, **237**, 786–791.
- 9 E. L. Zdorovenko, G. V. Zatonsky, G. M. Zdorovenko, L. A. Pasichnyk, A. S. Shashkov and Y. A. Knirel, *Carbohydr. Res.*, 2001, **336**, 329–336.
- 10 A. Turska-Szewczuk, A. Kozinska, R. Russa and O. Holst, *Carbohydr. Res.*, 2010, **345**, 680–684.
- 11 E. Sävén, J. Östervall, C. Landersjö, M. Edblad, A. Weintraub, M. Ansaruzzaman and G. Widmalm, *Carbohydr. Res.*, 2012, **348**, 99–103.



- 12 T. A. Chowdhury, B. Lindberg, U. Lindquist and J. Baird, *Carbohydr. Res.*, 1987, **164**, 117–122.
- 13 U. Olsson, K. Lycknert, R. Stenutz, A. Weintraub and G. Widmalm, *Carbohydr. Res.*, 2005, **340**, 167–171.
- 14 M. V. Svensson, A. Weintraub and G. Widmalm, *Carbohydr. Res.*, 2011, **346**, 2300–2303.
- 15 B. Coxon, N. Sari, G. Batta and V. Pozsgay, *Carbohydr. Res.*, 2000, **324**, 53–65.
- 16 B. Stevensson, C. Landersjö, G. Widmalm and A. Maliniak, *J. Am. Chem. Soc.*, 2002, **124**, 5946–5947.
- 17 E. Bedini, C. De Castro, G. Erbs, L. Mangoni, J. M. Dow, A.-M. Newman, M. Parrilli and C. Unverzagt, *J. Am. Chem. Soc.*, 2005, **127**, 2414–2416.
- 18 C. Landersjö, B. Stevensson, R. Eklund, J. Östervall, P. Söderman, G. Widmalm and A. Maliniak, *J. Biomol. NMR*, 2006, **35**, 89–101.
- 19 R. Eklund, K. Lycknert, P. Söderman and G. Widmalm, *J. Phys. Chem. B*, 2005, **109**, 19936–19945.
- 20 G. Lipari and A. Szabo, *J. Am. Chem. Soc.*, 1982, **104**, 4546–4559.
- 21 B. Coxon, *Adv. Carbohydr. Chem. Biochem.*, 2009, **62**, 17–82.
- 22 W. R. P. Scott, A. E. Mark and W. F. van Gunsteren, *J. Biomol. NMR*, 1998, **12**, 501–508.
- 23 O. Fiset, P. Lagüe, S. Gagné and S. Morin, *J. Biomed. Biotechnol.*, 2012, 254208.
- 24 K. H. M. Jonsson, E. Sävén and G. Widmalm, *Org. Biomol. Chem.*, 2012, **10**, 2453–2463.
- 25 P. Söderman and G. Widmalm, *Magn. Reson. Chem.*, 1999, **37**, 586–590.
- 26 M. Zerbetto, A. Polimeno, D. Kotsyubynskyy, L. Ghalebani, J. Kowalewski, E. Meirovitch, U. Olsson and G. Widmalm, *J. Chem. Phys.*, 2009, **131**, 234501.
- 27 M. Zerbetto, D. Kotsyubynskyy, J. Kowalewski, G. Widmalm and A. Polimeno, *J. Phys. Chem. B*, 2012, **116**, 13159–13171.
- 28 D. Kotsyubynskyy, M. Zerbetto, M. Soltesova, O. Engström, R. Pendrill, J. Kowalewski, G. Widmalm and A. Polimeno, *J. Phys. Chem. B*, 2012, **116**, 14541–14555.
- 29 H. Risken, *The Fokker-Planck Equation*, Springer-Verlag, Berlin, 2nd edn, 1989.
- 30 V. Barone, M. Zerbetto and A. Polimeno, *J. Comput. Chem.*, 2009, **30**, 2–13.
- 31 A. Polimeno and J. H. Freed, *J. Phys. Chem.*, 1995, **99**, 10995–11006.
- 32 M. Zerbetto, A. Polimeno and E. Meirovitch, *J. Phys. Chem. B*, 2009, **113**, 13613–13625.
- 33 Y.-Y. Chen, S.-Y. Luo, S.-C. Hung, S. I. Chan and D.-L. Tzou, *Carbohydr. Res.*, 2005, **340**, 723–729.
- 34 M. Zerbetto, A. Polimeno and E. Meirovitch, *Int. J. Quantum Chem.*, 2010, **110**, 387–405.
- 35 M. Findeisen, T. Brand and S. Berger, *Magn. Reson. Chem.*, 2007, **45**, 175–178.
- 36 P. Damberg, J. Jarvet and A. Gräslund, *J. Magn. Reson.*, 2001, **148**, 343–348.
- 37 R. Mills, *J. Phys. Chem.*, 1973, **77**, 685–688.
- 38 D. Canet, G. C. Levy and I. R. Peat, *J. Magn. Reson.*, 1975, **18**, 199–204.
- 39 S. Meiboom and D. Gill, *Rev. Sci. Instrum.*, 1958, **29**, 688–691.
- 40 F. del Río-Portilla, V. Blechta and R. Freeman, *J. Magn. Reson., Ser. A*, 1994, **111**, 132–135.
- 41 A. Garza-García, G. Ponzanelli-Velázquez and F. del Río-Portilla, *J. Magn. Reson.*, 2001, **148**, 214–219.
- 42 B. R. Brooks, C. L. Brooks III, A. D. MacKerell Jr, L. Nilsson, R. J. Petrella, B. Roux, Y. Won, G. Archontis, C. Bartels and S. Boresch, *et al.*, *J. Comput. Chem.*, 2009, **30**, 1545–1614.
- 43 O. Guvench, E. Hatcher, R. M. Venable, R. W. Pastor and A. D. MacKerell Jr, *J. Chem. Theory Comput.*, 2009, **5**, 2353–2370.
- 44 W. L. Jorgensen, J. Chandrasekhar, J. D. Madura, R. W. Impey and M. L. Klein, *J. Chem. Phys.*, 1983, **79**, 926–935.
- 45 M. L. Strader and S. E. Feller, *J. Phys. Chem. A*, 2002, **106**, 1074–1080.
- 46 S. Nosé, *Mol. Phys.*, 1984, **52**, 255–268.
- 47 W. G. Hoover, *Phys. Rev. A*, 1985, **31**, 1695–1697.
- 48 J.-P. Ryckaert, G. Ciccotti and H. J. C. Berendsen, *J. Comput. Phys.*, 1977, **23**, 327–341.
- 49 T. Darden, D. York and L. Pedersen, *J. Chem. Phys.*, 1993, **98**, 10089–10092.
- 50 I.-C. Yeh and G. Hummer, *J. Phys. Chem. B*, 2004, **108**, 15873–15879.
- 51 J. W. Eaton, D. Bateman and S. Hauberg, *GNU Octave Manual Version 3*, Network Theory Ltd, United Kingdom, 2008.
- 52 M. Chalaris, S. Marinakis and D. Dellis, *Fluid Phase Equilib.*, 2008, **267**, 47–60.
- 53 I. M. Svishchev and P. G. Kusalik, *J. Chem. Phys.*, 1993, **99**, 3049–3058.
- 54 A. Vishnyakov, A. Laaksonen and G. Widmalm, *J. Mol. Graphics Modell.*, 2001, **19**, 338–342, 396–397.
- 55 R. Pendrill, E. Sävén and G. Widmalm, *J. Phys. Chem. B*, 2013, **117**, 14709–14722.
- 56 W. B. O'Dell, D. C. Baker and S. E. McLain, *PLoS One*, 2012, **7**, e45311.
- 57 M. D. Battistel, R. Pendrill, G. Widmalm and D. I. Freedberg, *J. Phys. Chem. B*, 2013, **117**, 4860–4869.
- 58 T. Rundlöf, A. Kjellberg, C. Damberg, T. Nishida and G. Widmalm, *Magn. Reson. Chem.*, 1998, **36**, 839–847.
- 59 E. Sävén, T. Massad, C. Landersjö, P. Damberg and G. Widmalm, *Org. Biomol. Chem.*, 2010, **8**, 3684–3695.
- 60 B. J. Hardy, S. Bystricky, P. Kovac and G. Widmalm, *Biopolymers*, 1997, **41**, 83–96.
- 61 J. Kowalewski, L. Mäler and G. Widmalm, *J. Mol. Liq.*, 1998, **78**, 225–261.
- 62 M. Soltesova, J. Kowalewski and G. Widmalm, *J. Biomol. NMR*, 2013, **57**, 37–45.
- 63 J. Kowalewski and L. Mäler, *Nuclear spin relaxation in liquids: Theory, experiments, and applications*, CRC Press, Boca Raton, FL, 2006.
- 64 J. Xia and D. A. Case, *Biopolymers*, 2012, **97**, 289–302.
- 65 B. J. Hardy, W. Egan and G. Widmalm, *Int. J. Biol. Macromol.*, 1995, **17**, 149–160.
- 66 A. Kjellberg, T. Rundlöf, J. Kowalewski and G. Widmalm, *J. Phys. Chem. B*, 1998, **102**, 1013–1020.



- 67 E. R. Henry and A. Szabo, *J. Chem. Phys.*, 1985, **82**, 4753–4761.
- 68 J. Kowalewski, M. Effemey and J. Jokisaari, *J. Magn. Reson.*, 2002, **157**, 171–177.
- 69 E. Hatcher, E. Sävén, G. Widmalm and A. D. MacKerell Jr, *J. Phys. Chem. B*, 2011, **115**, 597–608.
- 70 A. M. Dixon, R. Venable, G. Widmalm, T. E. Bull and R. W. Pastor, *Biopolymers*, 2003, **69**, 448–460.
- 71 S. Bagley, H. Kovacs, J. Kowalewski and G. Widmalm, *Magn. Reson. Chem.*, 1992, **30**, 733–739.
- 72 A. Poveda, J. L. Asensio, M. Martín-Pastor and J. Jiménez-Barbero, *J. Biomol. NMR*, 1997, **10**, 29–43.
- 73 L. Mäler, J. Lang, G. Widmalm and J. Kowalewski, *Magn. Reson. Chem.*, 1995, **33**, 541–548.
- 74 A. Almond, J. Bunkenborg, T. Franch, C. H. Gotfredsen and J. Ø. Duus, *J. Am. Chem. Soc.*, 2001, **123**, 4792–4802.
- 75 L. Mäler, G. Widmalm and J. Kowalewski, *J. Biomol. NMR*, 1996, **7**, 1–7.
- 76 T. Rundlöf, R. M. Venable, R. W. Pastor, J. Kowalewski and G. Widmalm, *J. Am. Chem. Soc.*, 1999, **121**, 11847–11854.
- 77 E. Meirovitch, Y. E. Shapiro, A. Polimeno and J. H. Freed, *Prog. Nucl. Magn. Reson. Spectrosc.*, 2010, **56**, 360–405.
- 78 J. Kowalewski and G. Widmalm, *J. Phys. Chem.*, 1994, **98**, 28–34.

